

# Multi-Task Handwritten Document Layout Analysis

Lorenzo Quirós

**Abstract**—Document Layout Analysis is a fundamental step in Handwritten Text Processing systems, from the extraction of the text lines to the type of region where it belongs. We present a system based on artificial neural networks which is able to extract not only the baselines present in the document, but *geometric and logic layout analysis* of the document as well. Experiments in three different datasets demonstrate the potential of the method and show competitive results with state-of-the-art methods.

**Index Terms**—document layout analysis, text line detection, baseline detection, semantic segmentation, zone segmentation, handwritten text recognition



## 1 INTRODUCTION

HANDWRITTEN Text Processing (HTP) systems such as Handwritten Text Recognition (HTR) [1], Keyword Spotting (KWS) [2] and Information Retrieval for Handwritten Documents [3] are well known problems where an image of a handwritten document is used as an input and some kind of text-related information is expected as output. But for all current HTP systems, the image should only contain a handwritten sequence, this is only one *line* of handwritten text is processed at once. However, since the main goal of those systems is to process not just a single line, but the complete paragraph or even the complete document, a previous system is needed in order to segment those lines from the whole page and, in an upper level, to segment the different zones of the page (paragraph, marginal notes, illustrations, page number, etc.) in a meaningful manner (normally consistent with the reading order). Consequently, this is a very important stage of any HTP system.

Document Layout Analysis (DLA) is the process of identifying and categorizing the zones of interest in an image of a document. Commonly this process is divided into two sub problems [4]. First, *geometric layout analysis* aims at producing a description of the geometric structure of the document ( i.e. where each zone is placed, its shape and relationship with other zones). This structure allows us to describe the document layout at different levels of detail (e.g. a set of text lines can be viewed at higher level as a paragraph). Second, the classification of those zones into their logical role (title, paragraph, illustration, etc.) is called the *logical layout analysis*. Although, *logical layout analysis* is not necessary for zone segmentation nor for text line extraction it is a very important step necessary to present the results of HTP systems in the same context as the input document (e.g. the transcript of some text line can be presented as a title or other type only if the zone label is defined, otherwise we can just provide the plain transcript).

Therefore, the first subproblem is related to the requirement of current systems to have a segmented input (single line of text), and the second subproblem refers to the ability

of the system to present the results in the same context as the input.

Nowadays the determination of text lines has been focused in the detection of its baseline (the imaginary line upon which a line of text rests) instead of the detailed polygon surrounding the text line. Owing to the fact that a baseline is defined by only few points, humans can easily label text images without the cumbersome process of obtaining a fully segmented line. Also, once some DLA system provides a baseline for each line in a document it can be easily reviewed and corrected by the user. Besides, rough segmentation of a text line can be straightforwardly obtained from its baseline, and because state-of-the-art HTP systems are able to filter out a lot of noise present in the input this rough segmented lines can be used by the HTP system with almost no negative impact on performance [5].

It is very important to notice the huge impact the context provided by the *logical layout analysis* can have in the performance of HTP systems. For example a well segmented text line labeled as a part of the *page number* text zone is expected to have only digits; then the search space for the HTP system can be reduced drastically.

In this work, we present a system based on Artificial Neural Networks, which is able to detect the baselines, the zones and the label of those zones from the digital image of the document. It is an integrated approach, where baselines and text zones are detected and segmented in a single process, but the relationship between them is defined in a top-down way.

The rest of this paper is organized as follows. In Sec. 2 related work is discussed. Then, the proposed method is presented in Sec. 3. Afterwards, experimental setup is presented in Sec. 4, while results are reported in Sec. 5. Finally we draw some conclusions in Sec. 6.

## 2 RELATED WORK

Comprehensive surveys about document image analysis [6], [7], [8] and [9] provide a very good insight about the state-of-the-art algorithms for document segmentation, including document layout analysis for handwritten text documents.

*Author is member of the Pattern Recognition and Human Language Technology Research Center, Universitat Politècnica de València, Spain.  
E-mail: loquidia@prhlt.upv.es.*

In this work we focus on DLA algorithms for handwritten text documents.

DLA algorithms can be divided typologically by the problem they are developed to solve into three groups: text line extraction (included baseline detection), zone segmentation and zone labeling. Most of the methods focus on only one of these groups, or provide a separate algorithm for each one. In this work we present a method that encompasses all three groups under the same model.

## 2.1 Text line extraction

This is the group where most methods belong, mainly because of its direct applicability to HTP systems. The main goal of these methods is to segment the input image into a set of smaller images, each of which contains a single text line.

Methods such as those presented in [10], [11], [12], [13], [14] rely on connected components extraction after some filtering stage; [15], [16] methods rely on a tracer function to separate the different text lines after applying a blur to the input image. Other methods rely on Hidden Markov Models [17], [18], [19] or Recurrent Neural Networks [20] to model the vertical sequential structure of the text lines, or Convolutional Neural Networks [21] to classify between text line and non-text-line each pixel in the image.

## 2.2 Zone segmentation

Most of the methods for text line extraction rely on the assumption that input images contain a single region of text. This is, documents with a single column layout or images previously segmented into the different text zones. This group gathers the methods aiming to provide this level of segmentation.

Several methods are based on some kind of classifier (Multilayer Perceptron [14], [22], [23], [24], Conditional Random Fields [25], Definite Clause Grammars [26], Gaussian Mixture Models and Support Vector Machines [24]) whose input is a set of handcrafted features from the input images (Gabor filters, Kalman filters, Connected Components, Multi-scale images, etc). Others aim to provide an interactive framework to review the results of the zone segmentation algorithm [27].

## 2.3 Zone labeling

Although methods of this group are very related to methods of the previous group, some of them focus only on separating text from non-text zones [23], [24], [28] (which can be considered as a simplified form of Zone labeling), while others go forward to provide not just the segmentation of the zones but also the corresponding zone labels (three different zones are labeled on [25], two on [22] and six on [26]).

## 3 PROPOSED METHOD

An overview of the proposed method for Document Layout Analysis is given in Fig. 1. The method consists of two main stages. In the first stage an Artificial Neural Network (ANN) is used to classify the pixels of the input image ( $\mathbf{x}$ , with height  $h$ , width  $w$  and  $\gamma$  channels) into a set of zones of interest.

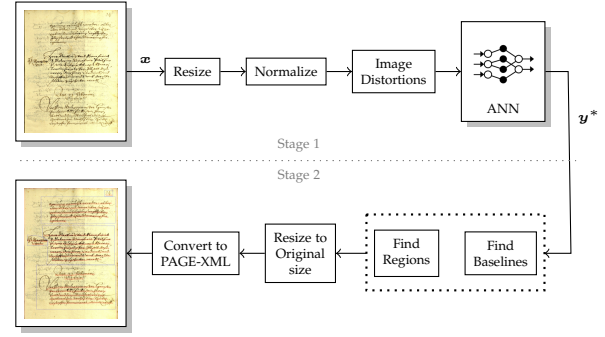


Fig. 1. Proposed method overview.  $\mathbf{x}$  is the input image and  $\mathbf{y}^*$  is the best hypothesis from the ANN.

In the second stage a detection algorithm is used to search for the baselines of each text line inside each zone. In this way we obtain the location and label of each zone, and the baselines they contain.

### 3.1 Stage 1: Pixel Level Classification

Layout Analysis can be defined as a Multi-Task Learning (MTL) problem [29] where two tasks are defined:

- *Task A*: Baseline detection.
- *Task B*: Zones segmentation and labeling.

*Task A* consists in obtaining the baseline of each text line present in the input image. This baseline is used to extract the sub-image of the text line and feed some HTP system. On the other hand, *Task B* consists in dividing those baselines into a different set of zones they belong to. For example, baselines which are members of the main paragraph will be grouped together into a zone, while the ones which are members of a marginal note will be grouped into another. Since each line belongs to a different context, that information can be used by the HTP system to provide more accurate hypotheses.

On a general manner we can define a multi-task variable<sup>1</sup>  $\mathbf{y} = [\mathbf{y}^1, \dots, \mathbf{y}^T]$ , where  $\mathbf{y}^t \in \mathcal{Y}^t = \{1, \dots, K^t\}$  is a matrix of  $w$  columns and  $h$  rows, with  $K^t \in \mathbb{N}_+$  being the finite number of values associated with the  $t$ -th task. Then, the solution of our MTL for some test instance  $\mathbf{x}$  is given as the following optimization problem:

$$\hat{\mathbf{y}} = \arg \max_{\mathbf{y}} p(\mathbf{y} | \mathbf{x}) \quad (1)$$

where the conditional distribution  $p(\mathbf{y} | \mathbf{x})$  is usually unknown and has to be estimated from the training data  $D = \{(\mathbf{x}_i, \mathbf{y}_i)\}_{i=1}^n = \{(\mathbf{X}, \mathbf{Y})\}$ .

In our specific two-task case ( $T = 2$ ), since *Task A* ( $t = 1$ ) is a binary classification problem, then  $K^1 = 2$  (background, baseline). Meanwhile, *Task B* ( $t = 2$ ) is a multi-class problem where  $K^2$  is equal to the number of different zones in the specific corpus, plus one for the background; normally, the number of zones is small (e.g.  $K^2 < 15$ ).

The conditional distribution  $p(\mathbf{y} | \mathbf{x})$  is estimated by a modified version of the Conditional Generative Adversarial Network presented in [30], where the generative network

<sup>1</sup> For convenience, each task will be represented mathematically as a superscript over the variables (e.g.  $v^t$ ).

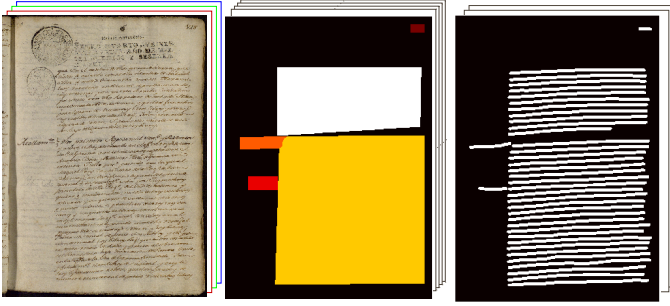


Fig. 2. Visualization of the encoded ground-truth to feed the ANN during training. From left to right: Original image ( $x$ ), *Task B* pixel-level ground-truth ( $y_2$ ), *Task A* pixel-level ground-truth ( $y_1$ ). The colors in the ground-truth images represent the position of the “1” in a 1-of- $K^t$  coding scheme. Better in color.

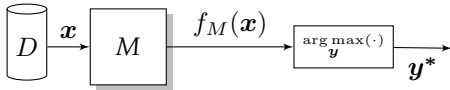


Fig. 3. Inference set-up for ANN.

output is replaced by a softmax layer for each task in the problem to ground the network to the underlying discriminative problem (this can be considered as a type of Discriminative Adversarial Network, as presented in [31]). The ANN is trained using labeled data as depicted in Fig. 2, where the color represent the position of the “1” in a 1-of- $K^t$  coding scheme.

### 3.1.1 ANN Inference

An ANN, called  $M$ , is trained to estimate the optimal solution of Eq. (1) (as depicted in Fig. 3), this is:

$$\mathbf{y}^* = \arg \max_{\mathbf{y}} f_M(\mathbf{x}) \quad (2)$$

where  $f_M(\cdot)$  is the output of the latest layer of the ANN  $M$ , and the  $\arg \max$  is computed element-wise. Notice this optimization problem can be considered as the trivial case (no restrictions), we are planning to add in a future version of the proposed method a set of restrictions such as the prior-probability of  $\mathbf{y}$  and structural restrictions in order to provide a more complete optimization problem.

### 3.1.2 ANN Objective

The objective function we want to minimize is composed of the interaction between two separated ANNs, that we call  $A$  and  $M$  networks. The  $A$  network is trained to distinguish between real labels (from  $D$ ) and generated labels (sometimes called fake labels) from  $M$  (notice  $A$  network is used only to help train  $M$ , and is discarded at inference time).

In the  $A$  network the cost function is the cross-entropy loss, where only two classes are defined, “1” when the input of the network belongs to the real labels, and “0” when the labels are generated by  $M$ , that is:<sup>II</sup>

$$\mathcal{L}_A(\mathbf{X}, \mathbf{Y}) = \frac{1}{2} \{ \mathcal{L}_A^1(\mathbf{X}, \mathbf{Y}) + \mathcal{L}_A^0(\mathbf{X}, \mathbf{Y}) \} \quad (3)$$

II. Parameters of the network are not shown explicitly in order to keep the notation as simple as possible.

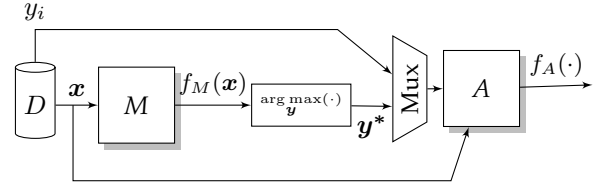


Fig. 4. Training set-up for ANN.

where

$$\mathcal{L}_A^1(\mathbf{X}, \mathbf{Y}) = \frac{-1}{n} \sum_{i=1}^n \{ \log f_A(\mathbf{x}_i | \mathbf{y}_i) \} \quad (4)$$

$$\mathcal{L}_A^0(\mathbf{X}, \mathbf{Y}) = \frac{-1}{n} \sum_{i=1}^n \log(1 - f_A(\mathbf{x}_i | \arg \max_{\mathbf{y}} f_M(\mathbf{x}_i))) \quad (5)$$

where  $\mathbf{x}_i | \mathbf{y}_i$  is the element-wise concatenation between  $\mathbf{x}_i$  and  $\mathbf{y}_i$ ,  $f_A(\cdot)$  is the output of the  $A$  network and  $f_M(\cdot)$  is the output of the  $M$  network. Hence  $\mathcal{L}_A(\mathbf{X}, \mathbf{Y})$  simplifies to

$$\begin{aligned} \mathcal{L}_A(\mathbf{X}, \mathbf{Y}) = & \frac{-1}{2n} \sum_{i=1}^n \left\{ \log f_A(\mathbf{x}_i | \mathbf{y}_i) \right. \\ & \left. + \log(1 - f_A(\mathbf{x}_i | \arg \max_{\mathbf{y}} f_M(\mathbf{x}_i))) \right\} \quad (6) \end{aligned}$$

On the other hand, the main network  $M$  performs the actual set of *Tasks* we aim at. In the  $M$  network the cost function is divided in two separated cost functions, whose trade-off is controlled by the hyperparameter  $\lambda$

$$\mathcal{L}_M(\mathbf{X}, \mathbf{Y}) = \frac{-1}{n} \sum_{i=1}^n \left\{ \mathcal{L}(\mathbf{x}_i, \mathbf{y}_i) + \lambda \mathcal{L}_A^0(\mathbf{x}_i, \mathbf{y}_i) \right\} \quad (7)$$

where  $\mathcal{L}_A(\cdot)$  drives the network to fool the network  $A$ , and  $\mathcal{L}(\mathbf{x}_i, \mathbf{y}_i)$  is the cross-entropy loss, which drives the network to learn the probability distribution of the training data:

$$\mathcal{L}(\mathbf{x}, \mathbf{y}) = \frac{-1}{Twh} \sum_{t=1}^T \left\{ \sum_{j=1}^{wh} \left\{ \sum_{c=1}^{K^t} \mathbf{y}_{j,c}^t \log(f_{M,c}^t(\mathbf{x}_j)) \right\} \right\} \quad (8)$$

where  $T$  is the number of *Tasks* to be performed,  $K^t$  is the number of classes of the task  $t \in T$ , the binary target variable  $\mathbf{y}_{j,c}^t \in \{0, 1\}$  have a 1-of- $K^t$  coding scheme indicating the correct class, and  $f_{M,c}^t(\mathbf{x}_j)$  is the output of the network  $M$  for the *Task*  $t$  and class  $c$ , interpreted as  $f_{M,c}^t(\mathbf{x}_j) = \text{p}(\mathbf{y}_{j,c}^t = 1 | \mathbf{x}_j)$  (i.e. the posterior probability of the pixel  $j$  of the input image belongs to the class  $c$  for task  $t$ ).

Both ANNs are optimized in parallel, following the standard approach from [32]: we alternate between one gradient descent step on  $M$ , then one step on  $A$ , and so on.

The training set-up is depicted in Fig. 4, where the “Mux” block is a standard multiplexer between the “real” label ( $\mathbf{y}_i$ ) and the “fake” one from the  $M$  network ( $\arg \max_{\mathbf{y}} f_M(\mathbf{x})$ ).

## 3.2 Stage 2: Zones Segmentation and baseline detection

### 3.2.1 Contour Extraction

Given a test instance  $x$  and its pixel level classification  $y^*$  obtained in the previous stage. First, the contour extraction algorithm presented by Suzuki et al. [33] is used for each zone over  $y^2$  to extract its contour. This algorithm provides a set of contours  $\Phi_k = \{\phi_1, \phi_2, \dots, \phi_R\}, k \in \mathcal{Y}^2, R \geq 0$ . Then, for each contour in  $\Phi_k$  the same extraction algorithm is used over  $y^1$  to find the contour where baselines are expected to be, but restricted to the area defined by the contour  $\phi_r, 1 \geq r \geq R$ . In this step, a new set of contours  $L_{k,r} = l_1, l_2, \dots, l_S; S \geq 0$  are found.

Finally each contour  $l_s, 0 \leq s \leq S$ , is supposed to contain a single line of text, whereby a simple baseline detection algorithm is applied to the section of the input image within the contour  $l_s$  (see Sec. 3.2.2).

Notice that *Task A* and *Task B* can be treated independently using the same formulation above by simply ignoring the network output associated to the task we are not interested in. Then, in Stage 2 we set the regions of interest to be only one with size equal to the input image, as defined in Eq. (9), to perform *Task A* only.

$$\Phi_k = \Phi_1 = \{\phi_1\}; \phi_1 = [(0, 0), (w, 0), (w, h), (0, h)] \quad (9)$$

Similarly, we just return  $\Phi_k, \forall k \in \mathcal{Y}^2$ , without further search inside those contours, to perform *Task B* alone.

### 3.2.2 Baseline detection algorithm

Once a text line contour  $l_s$  is detected, a very simple algorithm can be used to detect the baseline associated to that specific text line (under the assumption that there is only one text line per contour). Each baseline is represented as a piece-wise linear curve.

The pseudo code of the algorithm is presented on Alg. 1. First the input image  $x$  is cropped with the polygon defined in  $l_s$ , and it is binarized using Otsu's algorithm. Then, we define the lowest black pixel of each column in the binarized image as a point of the digital curve we are searching for. Finally, as a result of line 7, the number of points of the piece-wise linear curve  $\rho$  is equal to the number of columns of the cropped image  $Y$ . In order to reduce the number of points and remove some outliers, the algorithm presented by Perez et al. [34] to find an optimal piece-wise linear curve of only  $m$  vertices is used.

## 4 EXPERIMENTAL SET-UP

To assess the performance of the proposed method we test it on two publicly available datasets (cBAD<sup>III</sup> and Bozen<sup>IV</sup>), as well as on a new dataset called *Oficio de Hipotecas de Girona* (OHG).

OHG is a new dataset with the ground-truth annotated for baselines and several zones (segmentation and label), which will allow us to carry out a more detailed set of experiments in a dataset with a complex layout.

III. <https://zenodo.org/record/257972>

IV. <https://zenodo.org/record/218236>

---

### Algorithm 1: Baseline detection algorithm

---

**Data:** an image  $x$ , a contour  $l_s$ , number of vertex of output piece-wise linear curve  $m$

**Result:** piece-wise linear curve  $v$

```

1  $I = crop(x, l_s)$ 
2  $Y = Otsu(I)$ 
3  $\rho = []$ 
4 for  $i$  in  $rows(Y)$  do
5   for  $j$  in  $columns(Y)$  do
6     if  $Y_{i,j} == 1$  then
7        $\rho[j] = (j, i)$ 
8     end
9   end
10 end
11  $v = reducePoly(\rho, m)$ 

```

---

All experiments are conducted using the same hardware, a single NVIDIA TitanX GPU installed along with an Intel Core i5-2500K@3.30GHz CPU with 16GB RAM. The source code, along with the configuration files to replicate these experiments, are available at <https://github.com/lquiroso/P2PaLA>.

### 4.1 Ground-truth

Ground-truth is recorded in PAGE-XML format because it allow us to manually annotate and review the elements (baselines and zones) easily, as they can be defined by a piece-wise line or a polygon of just few points.

The ground-truth is then processed to encode the data into the one-hot encoding in order to train the ANNs. For each task in our MTL we have a pixel-level one-hot encoded matrix to feed the ANN and compute the respective loss function (Eq. 8). An example of the respective ground-truth is shown in Fig. 2, where each color represents a different value in the one-hot encoding.

### 4.2 Artificial Neural Network Architecture

As mentioned in Sec. 3.1, the proposed ANN architecture is very similar to the one presented by [30], but it was modified to perform a discriminative rather than a generative processing. The main hyper-parameters of each part of the ANN are presented below, following the convention presented in [30], where  $C_k$  denotes a Convolution-BatchNorm-LeakyReLU layer with  $k$  filters, and  $CD_k$  denotes a Convolution-BatchNorm-Dropout-ReLU layer with a dropout rate of 0.5.

#### 4.2.1 The A Network

This network is a simple single output Convolutional Neural Network, trained as explained in Sec. 3.1.2. Its main parameters are:

- number of input channels: defined by the number of channels of the input image (3 for RGB images) plus one more for each task involved. In the case of two tasks and RGB images number of input channels is 5.
- Architecture: C64-C128-C256-C512-C512-C512-Sigmoid.
- Convolution filters:  $4 \times 4$ , stride 2.

#### 4.2.2 The M Network

This network is structured as an encoder-decoder architecture called U-Net [35]. U-Net differs from a common encoder-decoder due its skip connections between each layer  $i$  in the encoder and layer  $n - i$  in the decoder, where  $n$  is the total number of layers. Main parameters are:

- number of input channels: defined by the number of channels of the input image (3 for RGB images).
- Architecture:
  - encoder: C64-C128-C256-C512-C512-C512, where ReLU layers are changed to LeakyReLU.
  - decoder: CD512-CD1024-CD1024-C1024-C1024-C512-C256-C128-SoftMax.
  - Convolution filters:  $4 \times 4$ , stride 2.

#### 4.2.3 Training and Inference

To optimize the networks we follow [30], using minibatch SGD and Adam solver [36], with a learning rate of 0.0001, and momentum parameters  $\beta_1 = 0.5$  and  $\beta_2 = 0.999$ . Also, we use weighted loss from [37], to overcome the imbalance problem in *Task B*. The weight is computed as  $w_k = \frac{1}{\log(c+p_k)}$ ,  $k \in \mathcal{Y}^t$ ,  $c \geq 0$ , where  $p_k$  is the prior-probability of the  $k$ -th value associated with the task.

Affine transformations (translation, rotation, shear, scale) and Elastic Deformations [38] are applied to the input images as a data augmentation technique, where its parameters are selected randomly from a restricted set of allowed values, and applied on each epoch and image with a probability of 0.5.

In our experiments, we use the maximum batch size allowed by the hardware we have available: 8 images of size  $1024 \times 768$  on a single Titan X GPU.

### 4.3 Evaluation Measures

#### 4.3.1 Baseline Detection

We report precision (P), recall (R) and its harmonic mean (F1) measures as defined in [39]. Tolerance parameters are set to default values in all experiments.

#### 4.3.2 Zone Segmentation

We report metrics from semantic segmentation and scene parsing evaluations as presented in [40]:

- Pixel accuracy (pixel acc.):  $\sum_i \eta_{ii} / \sum_i \tau_i$
- Mean accuracy (mean acc.):  $1/K^{t=2} \sum_i \eta_{ii} / \tau_i$
- Mean Jaccard Index (mean IU):  $(1/K^{t=2}) \sum_i \eta_{ii} / (\tau_i + \sum_j \eta_{ji} - \eta_{ii})$
- Frequency weighted Jaccard Index (f.w. IU):  $(\sum_{\kappa} \tau_{\kappa})^{-1} \sum_i \tau_i \eta_{ii} / (\tau_i + \sum_j \eta_{ji} - \eta_{ii})$

where  $\eta_{ij}$  is the number of pixels of class  $i$  predicted to belong to class  $j$ ,  $K^{t=2}$  is the number of different classes for the task  $t = 2$ ,  $\tau_i$  the number of pixels of class  $i$ , and  $\kappa \in \mathcal{Y}^{t=2}$ .

### 4.4 Data corpora

#### 4.4.1 Oficio de Hipotecas de Girona

The manuscript *Oficio de Hipotecas de Girona* (OHG) is provided by the Centre de Recerca d’Història Rural from the Universitat de Girona (CRHR)<sup>V</sup>. This collection is composed of hundreds of thousands of notarial deeds from the XVIII-XIX century (1768-1862). Sales, redemption of censuses, inheritance and matrimonial chapters are among the most common documentary typologies in the collection. This collection is divided in batches of 50 pages each, digitized at 300ppi in 24 bit RGB color, available as TIF images along with their respective ground-truth layout in PAGE XML format, compiled by the HTR group of the PRHLT<sup>VI</sup> center and CRHR. OHG pages are structured in a complex layout composed of six different zone types, namely: \$pag, \$tip, \$par, \$pac, \$not, \$nop; whose description is summarized in Table 1 and an example is depicted in Fig. 5.

TABLE 1  
Layout regions in the OHG dataset.

ID	Description
\$pag	page number.
\$tip	notarial typology.
\$par	a paragraph of text that begins next to a notarial typology.
\$pac	a paragraph that begins on a previous page.
\$not	a marginal note.
\$nop	a marginal note added a posteriori to the document.

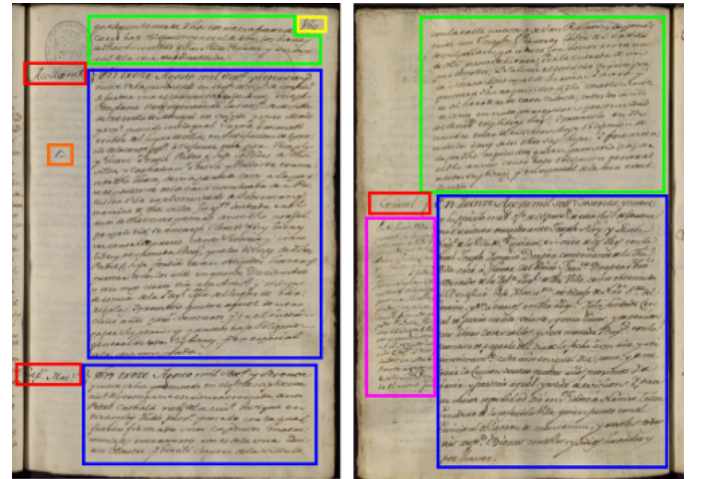


Fig. 5. Examples of pages with different layouts, belonging to the *Oficio de Hipotecas de Girona* dataset. Yellow: \$pag, red: \$tip, green: \$pac, blue: \$par, fuchsia: \$not, orange: \$nop (better seeing in color).

In this work we use a portion of 350 pages from the collection, from batch *b004* to batch *b010*. Main characteristics of this dataset are summarized on Table 2<sup>VII</sup>.

#### 4.4.2 cBAD dataset

This dataset is presented in [41] for the ICDAR 2017 Competition on Baseline Detection in Archival Documents (cBAD).

V. <http://www2.udg.edu/tabid/11296/Default.aspx>

VI. <https://prhlt.upv.es>

VII. The part of the corpus used in this paper will soon be available for research.

TABLE 2  
Main characteristics of the OHG dataset.

Batch	#Lines	#Zones					
		\$par	\$pac	\$tip	\$pag	\$nop	\$not
b004	1960	72	35	67	24	28	6
b005	1985	73	41	71	25	31	2
b006	1978	68	42	68	25	24	4
b007	1762	60	33	62	19	26	1
b008	1963	69	39	69	24	30	3
b009	1976	75	40	75	25	34	2
b010	2023	71	38	71	25	43	3
Total	13647	488	268	483	167	216	21

This dataset is composed of 2035 annotated document page images that are collected from 9 different archives. It is divided into two competition tracks to test different characteristics of the submitted methods. Track A [Simple Documents] is published with annotated text regions and therefore it test a method’s quality of text line segmentation (216 pages for training and 539 for test). The more challenging Track B [Complex Documents] provides only the page area (270 pages for training and 1010 for test). Hence, baseline detection algorithms need to correctly locate text lines in the presence of marginalia, tables, and noise. The dataset comprises images with additional PAGE XMLs. The PAGE XMLs contain text regions and baseline annotations.

#### 4.4.3 Bozen dataset

This dataset consists of a subset of documents from the Rat-protokolle collection composed of minutes of the council meetings held from 1470 to 1805 (about 30.000 pages). This dataset is written in Early Modern German. The number of writers is unknown. The public dataset is composed of 400 pages (350 for training and 50 for validation); most of the pages consist of a single block with many difficulties for line detection and extraction. The ground-truth in this set is in PAGE format and it is provided annotated at line level in the PAGE files [42].

## 5 RESULTS

### 5.1 Oficio de Hipotecas de Girona

The dataset is divided randomly into training and test set, 300 pages and 50 pages respectively. Experiments are conducted on incremental subsets from 16 to 300 training images, for *Task A* and *Task B*.

Two experiments are performed using this dataset. First, the system is configured to perform only *Task A* giving as result only the baselines present in the input images. Second, the system is configured to perform both tasks integrated, giving as result the baselines and the zones (segmentation and label).

Baseline results for both experiments are reported in Fig. 6. Even though there is statistically significant difference between the results of performing *Task A* alone and performing both tasks, this difference is admissible because of the benefit of having the zones segmented and labeled, especially when we have enough training images where the difference is small. Also, there is no appreciable impact in

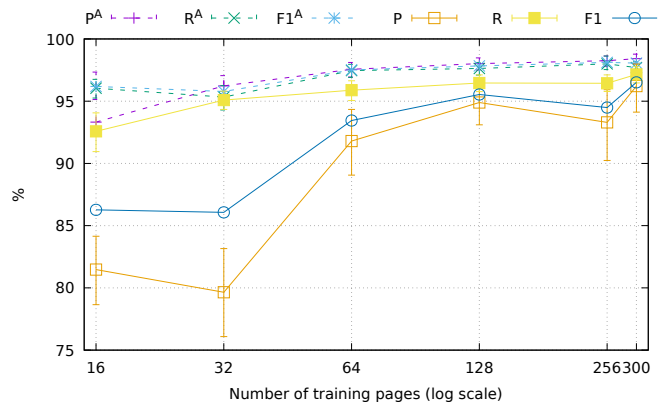


Fig. 6. Results for *Task A* of OHG. (·)<sup>A</sup> stands for results obtained only for *Task A* (i.e *Task B* is turned off). Better seeing in color.

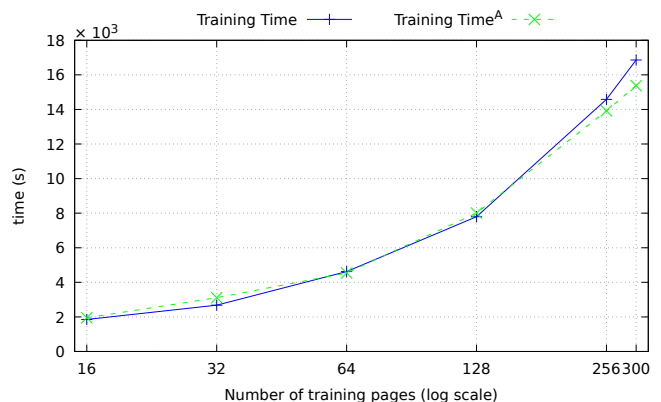


Fig. 7. Computing time required for OHG experiments. (·)<sup>A</sup> stands for results obtained only for *Task A* (i.e *Task B* is turned off). Better seeing in color.

the training time required by the system when we use two tasks or only one (see Fig. 7).

The recall measure obtained in both experiments is very stable across the number of training images, while precision is closely related to the quality of the zones segmented in the *Task B*, see Fig. 8 and 9.

Zone segmentation results are reported on Fig. 10. As expected an improvement due the increment of training images is observed until 128 images. There the results keep varying but without significant statistical difference.

### 5.2 cBAD

For this work, only Track B documents are used to train the system. The ground-truth of the test set is not available to the authors, whereby metrics are computed through the competition web site.

The system was trained through 200 epochs to perform *Task A* only, because no ground-truth is available for Text Zones in the dataset. Training time was around 3.75 hours using 270 training images on a mini-batch of 8.

Results are reported in Table 3, along with state-of-the-art results presented in the competition. The proposed approach achieved very competitive results on such a het-

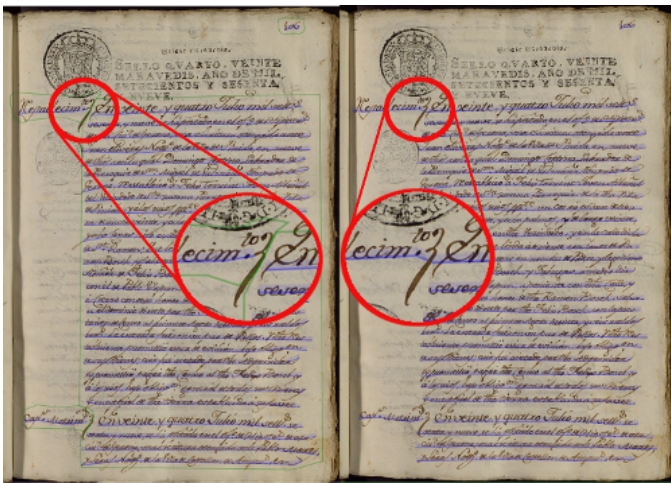


Fig. 8. Example of OHG results. In the left zone segmentation prevents the baselines to be merged (*Task A* and *B* are performed in an integrated manner). In the right the baselines are merged (*Task A* is performed alone). Better seeing in color.

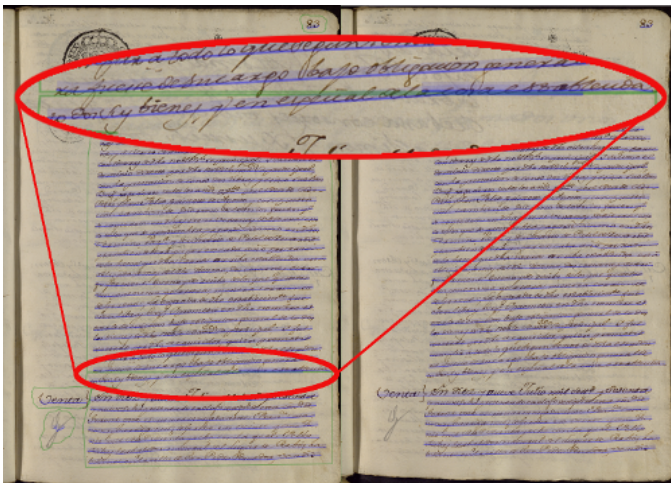


Fig. 9. Example of OHG results, where zone segmentation forces baseline to split. Left side is an example where *Task A* and *B* are performed, right side is an example when only *Task A* is performed. Better seeing in color.

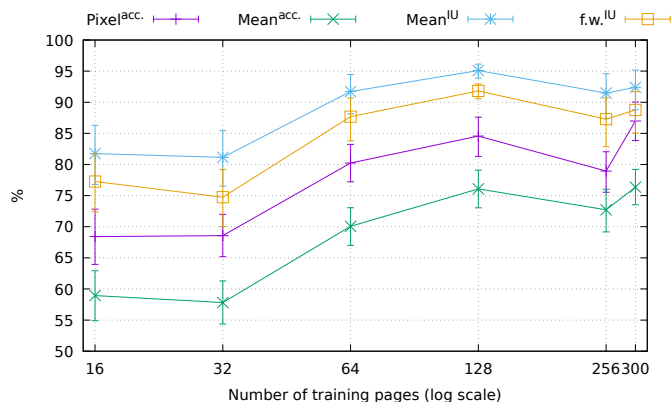


Fig. 10. Results for *Task B* of OHG. Better seeing in color.

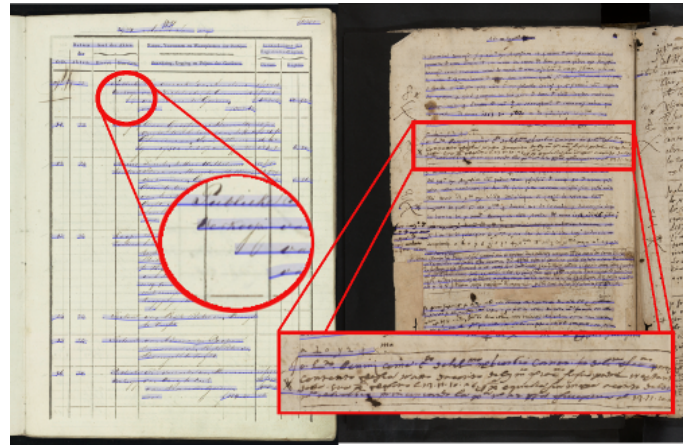


Fig. 11. Example of errors in cBAD results. Merged baselines are shown in the left, while missing baselines are showed in the right. Better seeing in color.

erogeneous dataset, without significant statistical difference with respect to the winner method of the competition<sup>VIII</sup>.

TABLE 3  
Results for the cBAD test set (*Task A* only). Nonparametric Bootstrapping confidence intervals at 95%, 10000 repetitions.

Method	P	R	F1
IRISA	69.2	77.2	73.0
UPVLC	83.3	60.6	70.2
BYU	77.3	82.0	79.9
proposed	84.8 [83.9, 85.7]	85.4 [84.4, 86.4]	85.1
DMRZ	85.4	86.3	85.9

Main errors are related to merged baselines or missing lines in very crowded areas. An example of those errors is shown in Fig. 11.

### 5.3 Bozen

Experiments on this work are conducted using the training/validation splits defined by the authors of the dataset, as training and test respectively.

The system was trained through 200 epochs to perform only *Task A*, because no ground-truth is available for Text Regions in the dataset. Training time was around 4.75 hours using 350 training images on a mini-batch of 8. Average inference time per page was 1.02s.

A F1 measure of 97.4 has been achieved<sup>IX</sup>, with 95.8 [92.7,97.8] precision and 99.1 [98.6, 99.4] recall<sup>X</sup>. An example of the results obtained in this corpus is shown in Fig. 12. These differences do not generally affect the results of HTP systems.

VIII. At the time this paper was being written a new result for this dataset was release as an arxiv pre-print [43], with a reported F1 higher (92.2) than the one reported here or in this competition.

IX. At the time this paper was being written a new result for this dataset was released as an arxiv pre-print [43], whose F1 reported (97.5) have no significant statistical difference with the results reported here.

X. Nonparametric Bootstrapping confidence intervals at 95%, 10000 repetitions.

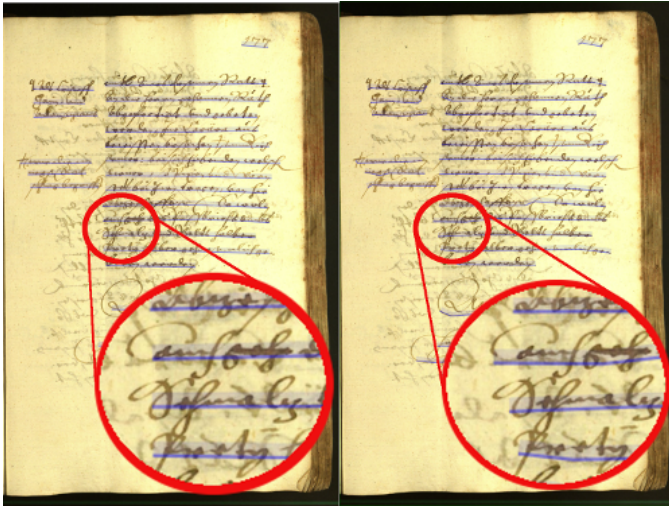


Fig. 12. Example of Bozen result. Left image is the ground-truth and at the right is the output of the system. Better seeing in color.

## 6 CONCLUSIONS

In this paper we present a new multi-task method for handwritten document layout analysis, which is able to perform zone segmentation and labeling along with baseline detection in an integrated way, using a single model. The method is based on discriminative ANN and a basic baseline detection algorithm.

We conducted experiments in three different datasets, with promising results on all of them without model reconstruction or hyper-parameter tuning.

Integrated model allow us to perform both tasks with the convenience of share (less parameters to be learned) and optimize (parameters are restricted to the loss in both tasks) the ANN parameters across tasks.

Baseline detection results in OHG and Bozen are good enough for most HTR and KWS applications, while cBAD results may not be enough for HTR applications where high quality transcripts are expected. In this sense, we will study the introduction of restrictions to the optimization problem, and the application of the Interactive Pattern Recognition framework established in [44] for layout analysis [27] to help users to easily review the document layout before feeding the HTP system.

## ACKNOWLEDGMENTS

The author would like to acknowledge Alejandro H. Toselli, Carlos-D. Martinez-Hinarejos and Enrique Vidal for their reviews and advice. Also, to NVIDIA Corporation for the donation of the Titan X GPU used for this research.

## REFERENCES

- [1] V. Romero, N. Serrano, A. H. Toselli, J. A. Sanchez, and E. Vidal, "Handwritten text recognition for historical documents," in *Proc. of the Workshop on Language Technologies for Digital Humanities and Cultural Heritage*, Hissar, Bulgaria, September 2011, pp. 90–96.
- [2] T. Bluche, S. Hamel, C. Kermorant, J. Puigcerver, D. Stutzmann, A. H. Toselli, and E. Vidal, "Preparatory kws experiments for large-scale indexing of a vast medieval manuscript collection in the himanis project," in *2017 14th IAPR International Conference on Document Analysis and Recognition (ICDAR)*, vol. 01, Nov 2017, pp. 311–316.
- [3] A. Fornés, V. Romero, A. Baró, J. I. Toledo, J. A. Sánchez, E. Vidal, and J. Lladós, "Icdar2017 competition on information extraction in historical handwritten records," in *Document Analysis and Recognition (ICDAR), 2017 14th IAPR International Conference on*, vol. 1. IEEE, 2017, pp. 1389–1394.
- [4] R. Cattoni, T. Coianiz, S. Messelodi, and C. M. Modena, "Geometric layout analysis techniques for document image understanding: a review," *ITC-irst, Tech. Rep.*, 1998.
- [5] V. Romero, J.-A. Sánchez, V. Bosch, K. Depuydt, and J. Does, "Influence of text line segmentation in handwritten text recognition," in *13th International Conference on Document Analysis and Recognition (ICDAR)*, 2015.
- [6] G. Nagy, "Twenty years of document image analysis in pami," *IEEE Transactions on Pattern Analysis and Machine Intelligence*, vol. 22, no. 1, pp. 38–62, Jan 2000.
- [7] S. Mao, A. Rosenfeld, and T. Kanungo, "Document structure analysis algorithms: a literature survey," in *Document Recognition and Retrieval X*, vol. 5010. International Society for Optics and Photonics, 2003, pp. 197–208.
- [8] A. M. Namboodiri and A. K. Jain, "Document structure and layout analysis," in *Digital Document Processing*. Springer, 2007, pp. 29–48.
- [9] S. Eskenazi, P. Gomez-Krämer, and J.-M. Ogier, "A comprehensive survey of mostly textual document segmentation algorithms since 2008," *Pattern Recognition*, vol. 64, pp. 1 – 14, 2017. [Online]. Available: <http://www.sciencedirect.com/science/article/pii/S0031320316303399>
- [10] Z. Shi, S. Setlur, and V. Govindaraju, "A steerable directional local profile technique for extraction of handwritten arabic text lines," in *10th International Conference on Document Analysis and Recognition (ICDAR)*, July 2009, pp. 176–180.
- [11] J. Ryu, H. I. Koo, and N. I. Cho, "Language-independent text-line extraction algorithm for handwritten documents," *IEEE Signal Processing Letters*, vol. 21, no. 9, pp. 1115–1119, Sept 2014.
- [12] N. Ouwayed and A. Belaïd, "A general approach for multi-oriented text line extraction of handwritten documents," *International Journal on Document Analysis and Recognition (IJ DAR)*, vol. 15, no. 4, pp. 297–314, Dec 2012. [Online]. Available: <https://doi.org/10.1007/s10032-011-0172-6>
- [13] R. Cohen, I. Dinstein, J. El-Sana, and K. Kedem, "Using scale-space anisotropic smoothing for text line extraction in historical documents," in *International Conference Image Analysis and Recognition*. Springer, 2014, pp. 349–358.
- [14] M. Baechler, M. Liwicki, and R. Ingold, "Text line extraction using dmlp classifiers for historical manuscripts," in *Document Analysis and Recognition (ICDAR), 2013 12th International Conference on*. IEEE, 2013, pp. 1029–1033.
- [15] N. Arvanitopoulos and S. Süsstrunk, "Seam carving for text line extraction on color and grayscale historical manuscripts," in *Frontiers in Handwriting Recognition (ICFHR), 2014 14th International Conference on*. IEEE, 2014, pp. 726–731.
- [16] A. Nicolaou and B. Gatos, "Handwritten text line segmentation by shredding text into its lines," in *10th International Conference on Document Analysis and Recognition (ICDAR)*, July 2009, pp. 626–630.
- [17] V. Bosch Campos, A. H. Toselli, and E. Vidal, "Natural language inspired approach for handwritten text line detection in legacy documents," in *Proceedings of the 6th Workshop on Language Technology for Cultural Heritage, Social Sciences, and Humanities*. Association for Computational Linguistics, 2012, pp. 107–111.
- [18] V. Bosch, A. H. Toselli, and E. Vidal, "Statistical text line analysis in handwritten documents," in *International Conference on Frontiers in Handwriting Recognition (ICFHR)*, Sept 2012, pp. 201–206.
- [19] —, "Semiautomatic text baseline detection in large historical handwritten documents," in *2014 14th International Conference on Frontiers in Handwriting Recognition*, Sept 2014, pp. 690–695.
- [20] B. Moysset, C. Kermorant, C. Wolf, and J. Louradour, "Paragraph text segmentation into lines with recurrent neural networks," in *2015 13th International Conference on Document Analysis and Recognition (ICDAR)*, Aug 2015, pp. 456–460.
- [21] J. Pastor-Pellicer, M. Z. Afzal, M. Liwicki, and M. J. Castro-Bleda, "Complete system for text line extraction using convolutional neural networks and watershed transform," in *2016 12th IAPR Workshop on Document Analysis Systems (DAS)*, April 2016, pp. 30–35.
- [22] S. S. Bukhari, T. M. Breuel, A. Asi, and J. El-Sana, "Layout analysis for Arabic historical document images using machine learning,"



- Proceedings - International Workshop on Frontiers in Handwriting Recognition (IWFHR)*, pp. 639–644, 2012.
- [23] M. Baechler and R. Ingold, “Multi resolution layout analysis of medieval manuscripts using dynamic mlp,” in *2011 International Conference on Document Analysis and Recognition*, Sept 2011, pp. 1185–1189.
- [24] H. Wei, M. Baechler, F. Slimane, and R. Ingold, “Evaluation of svm, mlp and gmm classifiers for layout analysis of historical documents,” in *2013 12th International Conference on Document Analysis and Recognition*, Aug 2013, pp. 1220–1224.
- [25] F. C. Fernández and O. R. Terrades, “Document segmentation using relative location features,” in *Proceedings of the 21st International Conference on Pattern Recognition (ICPR2012)*, Nov 2012, pp. 1562–1565.
- [26] A. Lemaitre, J. Camillerapp, and B. Coüasnon, “Multiresolution cooperation makes easier document structure recognition,” *International Journal of Document Analysis and Recognition (IJ DAR)*, vol. 11, no. 2, pp. 97–109, Nov 2008. [Online]. Available: <https://doi.org/10.1007/s10032-008-0072-6>
- [27] L. Quirós, C.-D. Martínez-Hinarejos, A. H. Toselli, and E. Vidal, “Interactive layout detection,” in *8th Iberian Conference on Pattern Recognition and Image Analysis (IbPRIA)*. Cham: Springer International Publishing, 2017, pp. 161–168.
- [28] G. Zhong and M. Cheriet, “Tensor representation learning based image patch analysis for text identification and recognition,” *Pattern Recognition*, vol. 48, no. 4, pp. 1211 – 1224, 2015. [Online]. Available: <http://www.sciencedirect.com/science/article/pii/S0031320314003938>
- [29] R. Caruana, “Multitask learning: A knowledge-based source of inductive bias,” in *Proceedings of the Tenth International Conference on Machine Learning*. Morgan Kaufmann, 1993, pp. 41–48.
- [30] P. Isola, J.-Y. Zhu, T. Zhou, and A. A. Efros, “Image-to-image translation with conditional adversarial networks,” *arxiv*, 2016.
- [31] C. N. dos Santos, K. Wadhawan, and B. Zhou, “Learning loss functions for semi-supervised learning via discriminative adversarial networks,” *CoRR*, vol. abs/1707.02198, 2017. [Online]. Available: <http://arxiv.org/abs/1707.02198>
- [32] I. Goodfellow, J. Pouget-Abadie, M. Mirza, B. Xu, D. Warde-Farley, S. Ozair, A. Courville, and Y. Bengio, “Generative adversarial nets,” in *Advances in Neural Information Processing Systems 27*, Z. Ghahramani, M. Welling, C. Cortes, N. D. Lawrence, and K. Q. Weinberger, Eds. Curran Associates, Inc., 2014, pp. 2672–2680. [Online]. Available: <http://papers.nips.cc/paper/5423-generative-adversarial-nets.pdf>
- [33] S. Suzuki *et al.*, “Topological structural analysis of digitized binary images by border following,” *Computer vision, graphics, and image processing*, vol. 30, no. 1, pp. 32–46, 1985.
- [34] J.-C. Perez and E. Vidal, “Optimum polygonal approximation of digitalized curves,” *Pattern Recognition Letters*, 1994.
- [35] O. Ronneberger, P. Fischer, and T. Brox, “U-net: Convolutional networks for biomedical image segmentation,” *CoRR*, vol. abs/1505.04597, 2015. [Online]. Available: <http://arxiv.org/abs/1505.04597>
- [36] D. P. Kingma and J. Ba, “Adam: A method for stochastic optimization,” *3rd International Conference on Learning Representations (ICLR)*, 2015.
- [37] A. Paszke, A. Chaurasia, S. Kim, and E. Culurciello, “Enet: A deep neural network architecture for real-time semantic segmentation,” *arXiv preprint arXiv:1606.02147*, 2016.
- [38] P. Y. Simard, D. Steinkraus, and J. Platt, “Best practices for convolutional neural networks applied to visual document analysis.” Institute of Electrical and Electronics Engineers, Inc., August 2003.
- [39] T. Grüning, R. Labahn, M. Diem, F. Kleber, and S. Fiel, “READ-BAD: A new dataset and evaluation scheme for baseline detection in archival documents,” *CoRR*, vol. abs/1705.03311, 2017. [Online]. Available: <http://arxiv.org/abs/1705.03311>
- [40] J. Long, E. Shelhamer, and T. Darrell, “Fully convolutional networks for semantic segmentation,” in *Proceedings of the IEEE conference on computer vision and pattern recognition*, 2015, pp. 3431–3440.
- [41] M. Diem, F. Kleber, S. Fiel, T. Gruning, and B. Gatos, “cbad: Icdar2017 competition on baseline detection,” in *2017 14th IAPR International Conference on Document Analysis and Recognition (ICDAR)*, vol. 01, Nov. 2017, pp. 1355–1360. [Online]. Available: [doi.ieeecomputersociety.org/10.1109/ICDAR.2017.222](https://doi.ieeecomputersociety.org/10.1109/ICDAR.2017.222)
- [42] J. A. Sánchez, V. Romero, A. H. Toselli, and E. Vidal, “Read dataset bozen,” Dec. 2016. [Online]. Available: <https://doi.org/10.5281/zenodo.218236>
- [43] T. Grüning, G. Leifert, T. Strauß, and R. Labahn, “A Two-Stage Method for Text Line Detection in Historical Documents,” *CoRR*, 2018. [Online]. Available: <http://arxiv.org/abs/1802.03345>
- [44] A. H. Toselli, E. Vidal, and F. Casacuberta, *Multimodal Interactive Pattern Recognition and Applications*. Heidelberg: Springer, 2011.